Dalton Transactions

ROYAL SOCIETY OF CHEMISTRY

PAPER

View Article Online
View Journal | View Issue

Cite this: *Dalton Trans.*, 2026, **55**, 2088

Iridium complexes of a chelating bis(iminoxolene): augmentation of metal–metal π bonding by metal–ligand π bonding

Kristin D. Grandstaff, Halen Carbonel and Seth N. Brown *

Received 19th October 2025,
Accepted 5th January 2026

DOI: 10.1039/d5dt02509e

rsc.li/dalton

Metalation of the *trans*-spanning 1,2-ethanediyldianthranilate-bridged bis(iminoquinone) $C_2H_4[O_2CC_6H_4$-2-$(NC_6H_2$-3,5-$^tBu_2$-2-$O)]_2$ (Egan) with bis(cyclooctene)iridium(I) chloride dimer results in the formation of a mixture of iridium compounds containing two, one or no chlorides per iridium. The monochloride product is a six-coordinate monomer, with one ester carbonyl of the bridge coordinated to give a *mer*, κ^3 iminoxolene linkage. This compound is formed exclusively as a *cis*-α isomer with the two iminoxolene nitrogens mutually trans, but it isomerizes upon heating to form an equilibrium mixture with the *cis*-β isomer. The iridium complex with no chlorides is iridium–iridium bonded dimeric (*A*,*C*)-$(Egan)_2Ir_2$, which is formed as a single S_4-symmetric stereoisomer. The iridium–iridium distance, 2.5584(4) Å, is extremely short for an unsupported iridium–iridium bond. This is attributed to donor–acceptor interactions between filled metal dπ orbitals on one iridium and empty metal–iminoxolene π* orbitals on the other iridium fostering a significant degree of metal–metal π bonding. The dimer can be reduced to a monomeric four-coordinate anion which is alkylated by iodomethane to form a five-coordinate methyliridium complex. In both of these complexes, the ester groups in the bridge are not bound to iridium.

Introduction

The iminoxolene ligand is a canonical example of a redox-active or "noninnocent" ligand, where the accessibility of the dianionic amidophenoxide, monoanionic iminosemiquinonate, and neutral iminoquinone gives rise to a rich coordination chemistry with metals across the periodic table.[1,2] The difference between the different oxidation states of the ligand corresponds to whether two, one, or zero electrons occupy the frontier molecular orbital of the iminoxolene, called the redox-active orbital (RAO), which consists of the in-phase combination of oxygen and nitrogen pπ orbitals interacting out of phase with a benzene π orbital (Fig. 1a). The C–O and C–N π* character of this orbital raises its energy relative to the usual energy of oxygen- or nitrogen-centered orbitals. This makes the energy close to that of the d orbitals of the middle transition metals, rendering the metal–iminoxolene bonding in these compounds highly covalent.[3,4] As a result, the oxidation states in these complexes are notoriously difficult to assign.[5] The out-of-phase combination of heteroatom p orbitals, called the subjacent orbital or SJO (Fig. 1b), is lower in energy but still close enough in energy to metal d orbitals to have a significant effect on bonding.[6]

Because of the tendency of iminoxolenes to dissociate under oxidative conditions,[7] there is good reason to explore poly(iminoxolene) ligands that use additional chelation to enhance metal binding. We recently reported the preparation of bis(aminophenol) ligands based on 1,2-ethanediyldianthranilate ($EganH_4$)[8] or (*R*,*R*)-2,3-butanediyldianthranilate ((*R*,*R*)-$BdanH_4$, Fig. 2a).[9] In contrast to bis(iminoxolene) ligands based on 2,2′-diaminobiphenyl[10] or 1,1′-bis(*p*-aminophenyl) ferrocene,[11] where the nitrogens must be bound in *cis* positions, the ligands derived from 1,2-ethanediyldianthranilate hold the nitrogens in trans positions in the square N_2O_2 framework in complexes such as (Egan)OsO or (Bdan)Pd (Fig. 2b). Metalations occur to form monomeric complexes in

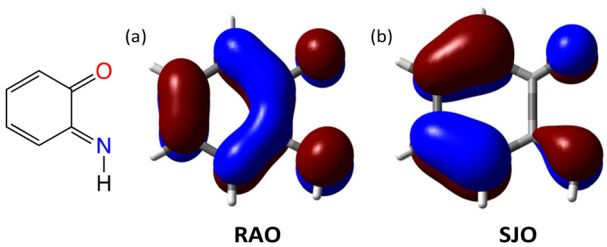

Fig. 1 Frontier orbitals of iminoxolene ligands. (a) Redox-active orbital or RAO (LUMO of iminoquinone). (b) Subjacent orbital or SJO (HOMO of iminoquinone).

Department of Chemistry and Biochemistry, University of Notre Dame, Notre Dame, IN 46556-5670, USA. E-mail: Seth.N.Brown.114@nd.edu

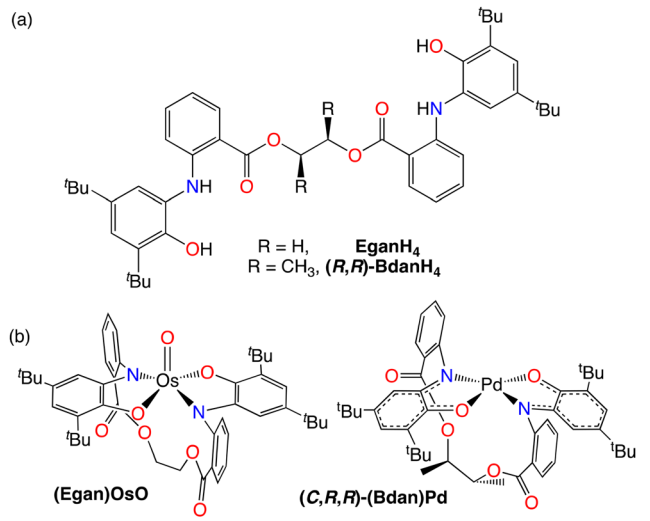

Fig. 2 *trans*-Spanning bis(iminoxolene) ligands. (a) Bis(aminophenol) ligands $EganH_4$ and (*R*,*R*)-$BdanH_4$. (b) Typical metal complexes showing the *trans*-N_2O_2 geometry and diastereoselective metal binding.

high yield with the alkanediyldianthranilate strap forming a 13-membered ring that lies over one face of the MN_2O_2 square plane, blocking it. With this face blocked, the metal atom is a chiral center, and the (*R*,*R*)-Bdan ligand transfers its chirality to provide optically active compounds with specifically a *C* configuration at the metal.[9]

We have prepared a number of bis(iminoxolene)iridium complexes[4,12] and have observed ligand substitution[13] and oxidative addition reactions of the complexes.[14] It would be interesting to explore the chemistry of iridium bonded to bis(iminoxolene) ligands such as Egan, but all existing Egan and Bdan complexes are prepared *via* the bis(aminophenol) ligands $EganH_4$ or $BdanH_4$, while routes to bis(iminoxolene)iridium or related complexes involve reactions of the iminoquinones with iridium(I) precursors such as $[(coe)_2IrCl]_2$ (coe = cyclooctene).

Here we report the oxidation of the bis(aminophenol) $EganH_4$ to the bis(iminoquinone) Egan and the metalation of the latter by $[(coe)_2IrCl]_2$. The products of metalation contain novel structural motifs: the complex *cis*-α-(Egan)IrCl features κ^5 binding, with one ester carbonyl oxygen bonded to iridium, and the complex (*A*,*C*)-$(Egan)_2Ir_2$ features two four-coordinate iridium centers joined by an unsupported iridium–iridium bond.

Experimental

General procedures

The bis(aminophenol) $EganH_4$ was prepared as described.[8] Deuterated solvents were obtained from Cambridge Isotope Laboratories. All other reagents were commercially available and used without further purification. NMR spectra were measured on a Bruker Avance DPX-400 or -500 spectrometer. Chemical shifts for ^1H and ^{13}C are reported in ppm downfield of TMS, with spectra referenced using the chemical shifts of the solvent residuals. Infrared spectra were measured as evaporated films on a Jasco 6300 FT-IR spectrometer or by ATR on a Bruker Alpha II FT-IR spectrometer housed in an inert atmosphere drybox. UV-visible spectra were measured as CH_2Cl_2 solutions in a 1 cm quartz cell on an Agilent 8453 diode array spectrophotometer. Cyclic voltammograms were performed using an Autolab potentiostat (PGSTAT 128N), with glassy carbon working and counter electrodes and a silver/silver chloride reference electrode. The electrodes were connected to the potentiostat through electrical conduits in the drybox wall. Samples were run with 0.1 M Bu_4NPF_6 as the electrolyte. Potentials were referenced to ferrocene/ferrocenium at 0 V (ref. 15) with the reference potential established by spiking the test solution with a small amount of decamethylferrocene (E° = −0.565 V *vs.* Cp_2Fe^+/Cp_2Fe in CH_2Cl_2 [16]). Elemental analyses were performed by Robertson Microlit (Ledgwood, NJ, USA).

Syntheses

1,2-Ethanediylbis(2-(2-oxo-3,5-di-*tert*-butyl-3,5-cyclohexadienylidenimino)benzoate), Egan. In the drybox, 1.6269 g $EganH_4$ (2.2948 mmol), 1.7142 g iodobenzene diacetate (5.3106 mmol, 2.3 equiv.), and 30 mL dry acetonitrile are added to a 100 mL round-bottom flask. After stirring at room temperature overnight, the flask is taken out into the air and the dark green precipitate is collected by suction filtration, washed with 20 mL acetonitrile and air-dried 15 min to yield 1.3518 g (59%) of the bis(iminoquinone). NMR spectroscopy indicates that the iminoquinone groups are a 3.4 : 1 mixture of *E* and *Z* isomers. ^1H NMR ($CDCl_3$), *E* isomer: δ 7.96 (d, 7.6 Hz, 2H, anthranilate H-6), 7.46 (t, 7.4 Hz, 2H, anthranilate H-4), 7.17 (t, 7.5 Hz, 2H, anthranilate H-5), 6.98 (s, 2H, iminoquinone CH), 6.66 (d, 7.8 Hz, 2H, anthranilate H-3), 6.00 (s, 2H, iminoquinone CH), 4.41 (s, 4H, OCH_2CH_2O), 1.31 (s, 18H, ^{t}Bu), 1.06 (s, 18H, ^{t}Bu). *Z* isomer: δ 7.99 (m obscured by *E* isomer, 2H, anthranilate H-6), 7.44 (m obscured by *E* isomer, 2H, anthranilate H-4), 7.06 (t, 7.4 Hz, 2H, anthranilate H-5), 6.94 (s, 2H, iminoquinone CH), 6.59 (s, 2H, iminoquinone CH), 6.50 (d, 7.9 Hz, 2H, anthranilate H-3), 4.39 (m, 4H, OCH_2CH_2O), 1.23 (s, 18H, ^{t}Bu), 1.13 (s, 18H, ^{t}Bu). $^{13}C\{^1H\}$ NMR (CD_2Cl_2), *E* stereoisomer: δ 184.09 (iminoquinone *C*═O), 165.55 (*C*OO), 156.42, 154.61, 152.45, 149.04, 134.65, 133.44, 131.71, 124.77, 119.85, 115.09, 63.17 (CH_2CH_2), 35.90 ($C[CH_3]_3$), 35.78 ($C[CH_3]_3$), 29.66 ($C[CH_3]_3$), 28.62 ($C[CH_3]_3$). *Z* stereoisomer: δ 180.32 (iminoquinone *C*═O), 165.73 (*C*OO), 156.12, 154.87, 153.88, 148.16, 134.92, 134.16, 125.04, 122.58, 120.26, 117.04, 62.79 (CH_2CH_2), 35.90 ($C[CH_3]_3$), 35.78 ($C[CH_3]_3$), 29.55 ($C[CH_3]_3$), 28.82 ($C[CH_3]_3$). IR (evapd film, cm^{-1}): 3066 (w), 2962 (s), 2870 (m), 1720 (s, ester $\nu_{C=O}$), 1667 (s, iminoquinone $\nu_{C=O}$), 1627 (m), 1595 (s), 1564 (m), 1475 (s), 1442 (m), 1375 (s), 1335 (w), 1280 (s), 1239 (s), 1200 (m), 1158 (m), 1129 (m), 1076 (s), 1044 (w), 969 (w), 896 (m), 865 (w), 802 (w), 758 (m), 736 (m), 706 (m). UV-vis (CH_2Cl_2): λ_{max} = 483 nm (sh, ε = 2140 L mol^{-1} cm^{-1}), 400 (6880). Anal. calcd for $C_{44}H_{52}N_2O_6$: C, 74.97; H, 7.44; N, 3.97. Found: C, 75.21; H, 7.25; H, 3.91.

Metalation of Egan with $[(coe)_2IrCl]_2$. In a typical run, 675.7 mg of Egan (0.959 mmol) and 493.8 mg of $[(coe)_2IrCl]_2$

(1.102 mmol Ir, 1.15 equiv.) are added to a 20 mL scintillation vial and suspended in 8 mL benzene in the drybox. A stir bar is added, and the reaction is stirred for 3 d at room temperature. The vial is removed from the drybox, and the solution is loaded onto a silica gel column and eluted with dichloromethane, which elutes both (*A*,*C*)-(Egan)$_2$Ir$_2$ and *cis*-α-(Egan)IrCl. The column is then flushed with 100% ethyl acetate, which elutes (Egan)IrCl$_2$. The dichloromethane eluate is evaporated to dryness on the rotary evaporator and then redissolved in 70 : 30 hexanes : ethyl acetate, loaded onto another silica gel column and eluted with the same solvent mixture. (*A*,*C*)-(Egan)$_2$Ir$_2$ elutes first with R_f = 0.96, followed by *cis*-α-(Egan)IrCl with R_f = 0.14. Each fraction is then stripped down on the rotary evaporator, slurried in pentane, filtered on a glass frit, washed with 10 mL pentane, and air dried for 10 min to give 188.8 mg (Egan)IrCl$_2$ (20%), 237.6 mg *cis*-α-(Egan)IrCl (27%) and 103.4 mg (*A*,*C*)-(Egan)$_2$Ir$_2$ (12%). The product distribution varies from batch to batch. **(Egan)IrCl$_2$**: IR (evapd film, cm^{-1}): 3069 (w), 2957 (m), 2907 (m), 2870 (w), 1722 (s, $\nu_{C=O}$), 1596 (m), 1523 (m). 1480 (m), 1444 (m), 1395 (w), 1353 (m), 1284 (s), 1252 (s), 1198 (s), 1177 (m), 1132 (m), 1090 (m), 1024 (m), 995 (m), 897 (w), 767 (w), 743 (m), 717 (w). UV-vis (CCl_4): 1980 nm (ε = 2000 L mol^{-1} cm^{-1}), 1653 (1100), 1368 (1280), 929 (1950), 737 (2080), 663 (2500), 411 (2540). Anal. calcd for $C_{44}H_{52}IrN_2O_6$: C, 54.59; H, 5.41; N, 2.89. Found: C, 55.45; H, 5.34; N, 2.75. ***cis*-α-(Egan)IrCl:** ^{1}H NMR (CD_2Cl_2): δ 8.21 (dd, 8.3, 1.6 Hz, 1H, anthranilate H-6), 7.99 (dd, 8.6, 0.6 Hz, 1H, anthranilate H-3), 7.80 (ddd, 8.7, 7.1, 1.6 Hz, 1H, anthranilate H-4), 7.74 (td, 7.8, 1.4 Hz, 1H, anthranilate H-4′), 7.67 (dd, 7.8, 1.4 Hz, 1H, anthranilate H-6′), 7.404 (d, 2.2 Hz, 1H, iminoxolene), 7.399 (td, 7.7, 1.1 Hz, 1H, anthranilate H-5′), 7.29 (dd, 8.0, 0.9 Hz, 1H, anthranilate H-3′), 7.25 (d, 2.0 Hz, 1H, iminoxolene), 7.06 (d, 2.0 Hz, 1H, iminoxolene), 6.89 (ddd, 8.4, 7.0, 1.0 Hz, 1H, anthranilate H-5), 6.69 (d, 2.1 Hz, 1H, iminoxolene), 5.50 (ddd, 12.6, 12.2, 2.0 Hz, 1H, IrOCOCH$_2$C*H*$_{ax}$CH$_{eq}$O), 4.69 (dt, 13.2, 1.5 Hz, 1H, IrOCOCH$_{ax}$C*H*$_{eq}$CH$_2$O), 4.39 (ddd, 13.1, 12.2, 2.6 Hz, 1H, IrOCOC*H*$_{ax}$CH$_{eq}$CH$_2$O), 4.16 (ddd, 13.0, 2.7, 1.2 Hz, 1H, IrOCOCH$_2$CH$_{ax}$C*H*$_{eq}$O), 1.29 (s, 9H, ^{t}Bu), 1.27 (s, 9H, ^{t}Bu), 1.03 (s, 9H, ^{t}Bu), 1.00 (s, 9H, ^{t}Bu). ^{13}C{^{1}H} NMR (CD_2Cl_2): δ 176.09, 174.58, 174.20, 168.18, 160.51, 153.32, 148.72, 148.00, 144.96, 141.60, 138.87, 137.22, 136.90, 134.56, 131.76, 130.97, 128.69, 127.93, 126.68, 122.81, 121.33, 120.64, 119.29, 116.63, 114.86, 111.03, 67.26 (*C*H$_2$), 66.29 (*C*H$_2$), 35.69 (*C*[CH$_3$]$_3$), 35.56 (*C*[CH$_3$]$_3$), 34.91 (*C*[CH$_3$]$_3$), 34.89 (*C*[CH$_3$]$_3$), 31.35 (C[*C*H$_3$]$_3$), 31.03 (C[*C*H$_3$]$_3$), 28.93 (C[*C*H$_3$]$_3$), 28.90 (C[*C*H$_3$]$_3$). IR (evapd film, cm^{-1}): 3060 (w), 2958 (s), 2907 (m), 2868 (m), 1738 (m, free $\nu_{C=O}$), 1598 (s), 1548 (w), 1524 (m), 1485 (m), 1466 (m), 1441 (m), 1394 (m), 1361 (m), 1336 (s), 1284 (m), 1261 (s), 1252 (s), 1221 (s), 1192 (s), 1173 (s), 1161 (s), 1108 (m). 1095 (m), 1050 (w), 1026 (m), 997 (m). UV-vis (CH_2Cl_2): 957 nm (ε = 6400 L mol^{-1} cm^{-1}), 490 (5300), 451 (6000 M^{-1} cm^{-1}). CV (CH_2Cl_2): −1.69, −0.97, 0.14, 0.65 V. Anal. calcd for $C_{44}H_{52}ClIrN_2O_6$: C, 56.67; H, 5.62; N, 3.00. Found: C, 56.18; H, 5.64; N 2.75. **(*A*,*C*)-(Egan)$_2$Ir$_2$**: ^{1}H NMR (C_6D_6): δ 7.76 (d, 2.1 Hz, 4H, iminoxolene), 7.41 (dd, 7.8, 1.5 Hz, 4H, anthranilate H-6), 7.36 (d, 2.0 Hz, 4H, iminoxolene), 6.93 (td, 7.5 Hz, 1.0 Hz, 4H, anthranilate H-4), 6.90 (dd, 8.3, 1.0 Hz, 2H, anthranilate H-3), 6.79 (td, 7.8 Hz, 1.5 Hz, 2H, anthranilate H-5), 3.36, 2.38 (m, J_{AB} = −12.4 Hz, $J_{AB'}$ = 1.8 Hz, $J_{AA'}$ = 11.6 Hz, $J_{BB'}$ = 2.3 Hz, 4H ea., OCH$_A$H$_B$CH$_{A'}$H$_{B'}$O), 1.41 (s, 36H, ^{t}Bu), 1.15 (s, 36H, ^{t}Bu). ^{13}C{^{1}H} NMR (CD_2Cl_2): δ 172.76 (iminoxolene *C*O), 167.69 (ester *C*=O), 156.09, 154.34, 141.16, 139.62, 131.24, 129.55, 129.11, 128.48, 127.28, 119.00, 113.17, 62.32 (O*C*H$_2$), 35.18 (*C*[CH$_3$]$_3$), 34.94 (*C*[CH$_3$]$_3$), 31.39 (C[*C*H$_3$]$_3$), 29.42 (C[*C*H$_3$]$_3$). IR (evapd film, cm^{-1}): 3070 (w), 2955 (s), 2869 (m), 1730 (s, $\nu_{C=O}$), 1597 (m), 1548 (m), 1548 (m), 1479 (m), 1445 (m), 1394 (m), 1362 (m), 1281 (s), 1252 (s), 1230 (s), 1199 (m), 1169 (m), 1132 (m), 1117 (m), 1095 (w), 1046 (w), 1027 (w), 1000 (w), 910 (w), 862 (w), 769 (w), 745 (m), 721 (w), 702 (w). UV-Vis (CH_2Cl_2): 940 nm (sh, ε = 3300 L mol^{-1} cm^{-1}), 895 (3400), 763 (sh, 10 100), 701 (15 800), 514 (7400), 488 (sh, 7200). Anal. calcd for $C_{88}H_{104}Ir_2N_4O_{12}$: C, 58.91; H, 5.84; N, 3.12. Found: C, 59.04; H, 6.27; N 2.87.

***cis*-β-(Egan)IrCl.** A solution of 92.1 mg of *cis*-α-(Egan)IrCl (0.204 mmol) in 4 mL of dry benzene is heated in a 60 °C oil bath under nitrogen for 3 d. The reaction mixture is cooled to room temperature, opened to the air, and loaded onto a plug of silica gel. Upon elution with 70 : 30 hexanes : ethyl acetate, *cis*-α-(Egan)IrCl elutes first (R_f = 0.14), followed by *cis*-β-(Egan)IrCl (R_f = 0.06). The *cis*-β-(Egan)IrCl product is slurried with hexanes, filtered on a glass frit, washed with 2 mL pentane, and air-dried for 10 min to give 29.8 mg *cis*-β-(Egan)IrCl (32%). ^{1}H NMR (C_6D_6): δ 7.75 (dd, 8.1, 1.5 Hz, 1H, anthranilate H-6), 7.36 (dd, 8.5, 0.6 Hz, 1H, anthranilate H-3), 7.12 (dd, 7.7, 1.4 Hz, 1H, anthranilate H-6), 7.04 (d, 2.1 Hz, 1H, iminoxolene), 6.94 (ddd, 8.7, 7.1, 1.6 Hz, 1H, anthranilate H-4), 6.78 (d, 2.1 Hz, 1H, iminoxolene), 6.69 (d, 2.0 Hz, 1H, iminoxolene), 6.66 (td, 7.6, 1.5 Hz, 1H, anthranilate H-4), 6.54 (td, 7.6, 1.2 Hz, 1H, anthranilate H-5), 6.21 (td, 8.1, 7.2, 0.9 Hz, 1H, anthranilate H-5), 5.84 (d, 2.1 Hz, 1H, iminoxolene), 5.25 (dd, 7.9, 1.0 Hz, 1H, anthranilate H-3), 4.99 (td, 12.3, 4.4 Hz, 1H, OCHH′CH″*H*‴O), 3.85 (dd, 11.3, 4.6 Hz, 1H, OCH*H*′CH″H‴O), 2.98 (td, 12.1, 5.1 Hz, 1H, OC*H*H′CH″H‴O), 2.74 (dd, 12.0, 5.1 Hz, 1H, OCHH′C*H*″H‴O), 1.91 (s, 9H, 6-^{t}Bu), 1.34 (s, 9H, 6-^{t}Bu), 1.33 (s, 9H, 4-^{t}Bu), 1.09 (s, 9H, 4-^{t}Bu). ^{13}C{^{1}H} NMR (CD_2Cl_2): δ 187.93 (IrO=*C*), 173.19 (iminoxolene *C*O), 172.79 (iminoxolene *C*O), 165.08 (free *C*=O), 159.49, 154.37, 150.12, 148.50, 141.21, 140.17, 139.77, 136.71, 135.98, 134.33, 131.59, 129.93, 129.64, 128.99, 127.84, 127.22, 119.91, 119.15, 118.65, 117.36, 116.13, 110.29, 63.73 (O*C*H$_2$C′H$_2$O), 61.18 (OCH$_2$*C*′H$_2$O), 35.93 (*C*[CH$_3$]$_3$), 35.79 (*C*[CH$_3$]$_3$), 34.71 (*C*[CH$_3$]$_3$), 34.63 (*C*[CH$_3$]$_3$), 31.75 (C[*C*H$_3$]$_3$), 31.50 (C[*C*H$_3$]$_3$), 29.86 (C[*C*H$_3$]$_3$), 28.74 (C[*C*H$_3$]$_3$). IR (evapd film, cm^{-1}): 2953 (s), 2870 (m), 1746 (m, $\nu_{C=O}$ free), 1594 (s, $\nu_{C=O}$ bound), 1581 (m), 1522 (m), 1481 (m), 1466 (m), 1439 (m), 1394 (m), 1361 (m), 1334 (s), 1305 (s), 1254 (s), 1222 (m), 1195 (s), 1175 (m), 1163 (m), 1125 (w), 1108 (m), 1096 (s), 1027 (m), 998 (m), 956 (w), 925 (w), 903 (w), 889 (w), 877 (w), 861 (w), 851 (w), 825 (w), 803 (w), 770 (w), 743 (m), 716 (w), 699 (w), 671 (w), 656 (w), 645 (w). UV-Vis (CH_2Cl_2): 930 nm (ε = 8500 L mol^{-1} cm^{-1}), 514 (7300), 460 (9300), 362 (9100), 336 (9600). CV (CH_2Cl_2): −0.93, 0.18, 0.67 V.

[Cp$_2$Co][(Egan)Ir]. In the drybox, 67.0 mg of (Egan)$_2$Ir$_2$ (0.0373 mmol) and 16.0 mg of cobaltocene (0.0846 mmol, 2.3

equiv.) are dissolved in 2 mL of dry THF in a scintillation vial. The vial is shaken and the reaction is left to stand at room temperature overnight. The mixture is filtered on a glass frit and dried under vacuum for 10 min to afford 55.6 mg (76%) of [Cp_2Co][(Egan)Ir]. ^{1}H NMR (acetone-d_6): δ 8.15 (dd, 8.1, 1.1 Hz, 2H, anthranilate H-3), 7.83 (td, 7.6 Hz, 1.5 Hz, 2H, anthranilate H-4), 7.65 (dd, 7.7 Hz, 1.5 Hz, 2H, anthranilate H-6), 7.27 (td, 7.6 Hz, 1.2 Hz, anthranilate H-5), 6.85 (d, 2.3 Hz, 2H, iminoxolene), 6.21 (d, 2.3 Hz, 2H, iminoxolene), 5.54 (s, 10H, Cp_2Co^+), 3.77, 3.26 (m, J_{AB} = −12.5 Hz, $J_{AB'}$ = 1.7 Hz, $J_{AA'}$ = 11.1 Hz, $J_{BB'}$ = 2.8 Hz, 2H ea., $OCH_AH_BCH_{A'}H_{B'}O$), 1.84 (s, 18H, ^{t}Bu), 1.11 (s, 18H, ^{t}Bu). ^{13}C{^{1}H} NMR (acetone-d_6): δ 172.43 (iminoxolene *C*O), 168.41 (ester *C*═O), 157.74, 148.07, 137.36, 133.68, 132.74, 132.65, 131.06, 129.58, 124.79, 114.93, 111.07, 85.87 (Cp_2Co^+), 62.23 (O*C*H_2), 35.98 (*C*[CH_3]$_3$), 34.41 (*C*[CH_3]$_3$), 32.51 (C[*C*H_3]$_3$), 31.29 (C[*C*H_3]$_3$). IR (ATR, cm^{-1}): 3085 (w), 2948 (m), 2902 (w), 2862 (w), 1721 (s, $\nu_{C=O}$), 1595 (w), 1472 (w), 1445 (m), 1412 (s), 1358 (w), 1304 (m), 1279 (m), 1255 (m), 1231 (m), 1202 (w), 1120 (w), 1077 (w), 1028 (w), 999 (m), 930 (w), 895 (w), 858 (s), 770 (m), 745 (m), 718 (m), 662 (w), 626 (m), 614 (w), 545 (w), 500 (m), 455 (vs). UV-Vis (acetone): 762 nm (sh, 1800 L mol^{-1} cm^{-1}), 659 (7950), 615 (7500), 377 (sh, 4300). Anal. calcd for $C_{54}H_{62}CoIrN_2O_6$: C, 59.71; H, 5.75; N, 2.58. Found: C, 58.21: H, 5.73; N, 2.23.

(Egan)IrCH$_3$. In the drybox, 217.9 mg of *cis*-α-(Egan)IrCl (0.234 mmol) and 136.5 mg of cobaltocene (0.722 mol, 3.1 equiv.) are dissolved in 10 mL dry acetone in a 20 mL scintillation vial. The reaction mixture is stirred for 10 min before 45 μL of iodomethane (0.723 mmol, 3.1 equiv.) is added. After stirring overnight, the solution is exposed to the air and the solvent removed on a rotary evaporator. The residue is dissolved in 5 mL dichloromethane and eluted through a silica plug with CH_2Cl_2. The dark purple fraction is collected and the solvent evaporated on the rotary evaporator. The residue is slurried in 4 mL pentane, suction filtered on a glass frit, and air-dried for 10 min to afford 76.8 mg (36% yield) of (Egan)IrCH$_3$. ^{1}H NMR (CD_2Cl_2): δ 8.46 (dd, 8.0, 1.4 Hz, 2H, anthranilate H-6), 7.79 (td, 7.6, 1.5 Hz, 2H, anthranilate H-4), 7.55 (ddd, 7.9, 7.3, 1.1 Hz, 2H, anthranilate H-5), 7.31 (dd, 8.0, 1.0 Hz, 2H, anthranilate H-3), 6.68 (d, 2.1 Hz, 2H, iminoxolene), 6.66 (d, 2.0 Hz, 2H, iminoxolene), 3.92 (2H, $CH_AH_BCH_{A'}H_{B'}$, J_{AB} = −12.35 Hz, $J_{AB'}$ = 1.55 Hz, $J_{AA'}$ = 10.50 Hz, $J_{BB'}$ = 3.40 Hz), 3.69 (2H, $CH_AH_BCH_{A'}H_B$), 1.92 (s, 3H, Ir*C*H_3), 1.24 (s, 18H, ^{t}Bu), 1.23 (s, 18H, ^{t}Bu). ^{13}C{^{1}H} NMR (CD_2Cl_2): δ 179.62 (iminoxolene *C*O), 166.38 (*C*═O), 151.09, 150.17, 139.45, 136.57, 133.60, 133.10, 129.08, 128.78, 127.24, 123.34, 112.57, 63.08 (O*C*H_2), 35.39 (*C*[CH_3]$_3$), 34.83 (*C*[CH_3]$_3$), 31.49 (C[*C*H_3]$_3$), 29.63 (C[*C*H_3]$_3$), −22.70 (Ir*C*H_3). IR (evapd film, cm^{-1}): 3069 (w), 2954 (s), 2904 (m), 2868 (m), 1716 (s, $\nu_{C=O}$), 1596 (m), 1543 (m), 1479 (m), 1446 (m), 1395 (w), 1361 (m), 1314 (m), 1280 (s), 1229 (s), 1196 (s), 1174 (s), 1114 (s), 1086 (m), 1026 (m), 1002 (m), 954 (w), 931 (w), 907 (w), 879 (w), 856 (w), 770 (w), 745 (m), 702 (w), 648 (w). UV-Vis (CH_2Cl_2): λ_{max} = 785 (51 000 L mol^{-1} cm^{-1}), 583 (4200), 462 (2600). CV (CH_2Cl_2): −2.20, −1.36, 0.09, 0.62. Anal. calcd for $C_{45}H_{55}IrN_2O_6$: C, 59.25; H, 6.08; N, 3.07. Found: C, 58.95; H, 5.94; N 3.08.

Computational methods

Calculations were performed on gas-phase compounds using either the egan ligand (Egan with *tert*-butyl groups replaced by hydrogen atoms) or the Hap ligand (Hap = 1,2-C_6H_4(O)(NH)). Geometries were optimized using hybrid density functional theory (B3LYP, SDD basis set for iridium and a 6-31G* basis set for all other atoms), using the Gaussian16 suite of programs.[17] The structures of *cis*-α-(egan)IrCl, *cis*-β-(egan)IrCl, and (*A*,*C*)-(Hap)$_4$Ir$_2$ (S_4-symmetry) were confirmed as minima by calculation of vibrational frequencies, while the structure of (*A*,*C*)-(Hap)$_4$Ir$_2$ constrained to C_{2h} symmetry was found to be a first-order saddle point with one imaginary frequency. Reported vibrational frequencies have been scaled by a factor of 0.9614.[18] Plots of calculated Kohn–Sham orbitals were generated using Gaussview (v. 6.0.16) with an isovalue of 0.04.

X-ray crystallography

Crystals were placed in inert oil before transferring to the N_2 cold stream of a Bruker Apex II CCD diffractometer. Data were reduced, correcting for absorption, using the program SADABS. Calculations used SHELXTL (Bruker AXS),[19] with scattering factors and anomalous dispersion terms taken from the literature.[20]

In *cis*-α-(Egan)IrCl·0.5CH_2Cl_2, the *tert*-butyl group centered at C18 was disordered in two orientations that shared a common carbon atom (C181). Corresponding carbon atoms in the two components were constrained to have the same thermal parameters and the occupancy allowed to refine, converging to 60.6(5)% occupancy for the major component. The lattice dichloromethane was disordered around an inversion center and was refined with occupancy fixed at 0.5. In (Egan)$_2$Ir$_2$·C_6H_6, after refinement of the iridium complex, there was a band of electron density around a $\bar{4}$ site in the lattice apparent on difference Fourier maps. This refined satisfactorily as a benzene molecule, with all carbons constrained to have the same thermal parameters and the molecule restrained to have C–C distances of 1.39 Å and to be planar, with estimated standard deviations of 0.02 Å. In [Cp_2Co][(Egan)Ir]·2.5THF, one of the lattice THF molecules was refined by restraining the C–O distances to 1.43 Å and the C–C distances to 1.52 Å. In (Egan)IrCH$_3$·2CH_2Cl_2, the two lattice solvents were disordered in two orientations, which were refined by constraining the thermal parameters of corresponding atoms in the two components to be equal and allowing the occupancies to refine. One *tert*-butyl group was found to be disordered in this structure, and initial refinement of the occupancy of the major component converged to 0.502(4), so the occupancy was fixed at 0.5 in the final refinement. Hydrogen atoms were generally found on difference Fourier maps and refined isotropically, with the exception of those on the disordered *tert*-butyl groups and lattice solvents, which were placed in calculated positions, as were all hydrogens in (Egan)$_2$Ir$_2$·C_6H_6. Hydrogens in calculated positions were refined with their isotropic thermal parameters tied to the

atom to which they were attached (1.5× for CH_3 groups, 1.2× for all others). Further details about the structures are in Tables 1 and 2.

Results and discussion

Synthesis and metalation of the ethanediyldianthranilate-bridged bis(iminoquinone) Egan

Iminoquinones are generally prepared by either carboxylic acid-catalyzed condensation of an aniline with 3,5-di-*tert*-butyl-1,2-benzoquinone[22] or oxidation of pre-formed 2-(*N*-arylamino)-4,6-di-*tert*-butylphenol.[23] Attempted reaction of the di-*tert*-butylbenzoquinone with ethylene glycol dianthranilate in neat acetic acid failed, with low conversion observed at room temperature and decomposition observed upon heating. This is consistent with observations that electron-withdrawing groups on the aniline hinder this condensation.[12,28] In contrast, oxidation of the bis(aminophenol) $EganH_4$ with iodobenzene diacetate proceeds smoothly to yield the bis(iminoquinone) (eqn (1)), with the iminoquinone groups observed as a 3.4 : 1 mixture of *E* and *Z* isomers in $CDCl_3$ solution. The ester carbonyl stretch in the IR shifts from 1694 cm^{-1} in $EganH_4$ [8] to 1720 cm^{-1} in the iminoquinone Egan, with the increase in frequency presumably due to both the loss of the NH–O hydrogen bond and the decrease in the electron-donating character of the *ortho* substituent from the arylamino group to the iminoquinone.

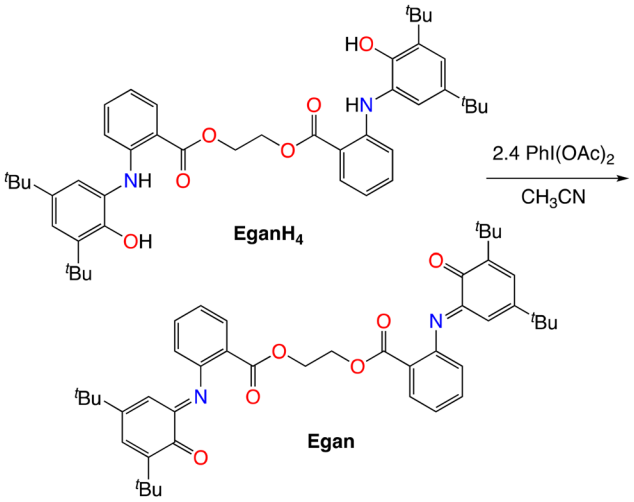

(1)

The iridium(I) complex $[(coe)_2IrCl]_2$ (coe = cyclooctene) reacts with Egan in benzene at room temperature under a nitrogen atmosphere. Consumption of the iminoquinone is immediate, but the product distribution slowly evolves. After three days, the reaction mixture contains a paramagnetic product and two major diamagnetic products (eqn (2)), which

Table 1 Summary of crystal data

	cis-α-(Egan)IrCl·0.5CH_2Cl_2	*cis*-β-(Egan)IrCl·$(CH_3)_2CO$	(*A*,*C*)-$(Egan)_2Ir_2·C_6H_6$	$[Cp_2Co][(Egan)Ir]·2.5THF$	(Egan)$IrCH_3·2CH_2Cl_2$
Molecular formula	$C_{44.5}H_{53}Cl_2IrN_2O_6$	$C_{47}H_{58}ClIrN_2O_7$	$C_{94}H_{110}Ir_2N_4O_{12}$	$C_{64}H_{82}CoIrN_2O_{8.5}$	$C_{47}H_{59}Cl_4IrN_2O_6$
Formula weight	974.99	990.60	1872.25	1266.44	1081.96
T/K	120(2)	120(2)	120(2)	120(2)	120(2)
Crystal system	Triclinic	Triclinic	Tetragonal	Orthorhombic	Triclinic
Space group	$P\bar{1}$	$P\bar{1}$	$P\bar{4}2_1c$	*Pbcn*	$P\bar{1}$
λ/Å	0.71073 (Mo Kα)	1.54178 (Cu Kα)	1.54178 (Cu Kα)	1.54178 (Cu Kα)	0.71073 (Mo Kα)
Total data collected	68 156	107 116	98 544	566 465	87 887
No. of indep reflns	10 495	9270	4317	11 980	8664
R_{int}	0.1203	0.1507	0.0517	0.1483	0.1218
Obsd refls [$I > 2\sigma(I)$]	8321	7832	3754	10 475	7447
a/Å	10.7868(6)	10.0999(3)	13.9570(10)	22.6380(19)	9.4851(3)
b/Å	14.0771(6)	14.1374(4)	13.9570(10)	19.1554(16)	15.5602(6)
c/Å	15.4091(8)	16.4491(5)	21.620(2)	27.048(2)	17.2975(6)
α/°	112.378(2)	99.418(2)	90	90	110.9286(12)
β/°	96.104(2)	94.139(2)	90	90	93.6788(12)
γ/°	97.621(2)	100.769(2)	90	90	95.5073(14)
V/Å^3	2112.88(19)	1661.61(10)	4211.5(7)	11 729.1(17)	2360.16(14)
Z	2	2	2	8	2
μ/mm^{-1}	3.335	6.661	6.537	6.994	3.103
Crystal size/mm	0.20 × 0.08 × 0.06	0.08 × 0.06 × 0.05	0.12 × 0.11 × 0.07	0.10 × 0.07 × 0.07	0.13 × 0.05 × 0.04
No. refined params	693	755	264	970	664
R_1, wR_2 [$I > 2\sigma(I)$]	R_1 = 0.0412 wR_2 = 0.0704	R_1 = 0.0290 wR_2 = 0.0540	R_1 = 0.0189 wR_2 = 0.0462	R_1 = 0.0248 wR_2 = 0.0462	R_1 = 0.0356 wR_2 = 0.0684
R_1, wR_2 [all data]	R_1 = 0.0658 wR_2 = 0.0768	R_1 = 0.0427 wR_2 = 0.0573	R_1 = 0.0239 wR_2 = 0.0489	R_1 = 0.0299 wR_2 = 0.0645	R_1 = 0.0478 wR_2 = 0.0722
Goodness of fit	1.043	1.008	1.084	1.042	1.026

Table 2 Selected distances, angles, and metrical oxidation states (MOS)[21] of iminoxolene ligands of structurally characterized compounds

	cis-α-(Egan)IrCl		*cis*-β-(Egan)IrCl		$(Egan)_2Ir_2$	$[Cp_2Co][(Egan)Ir]$	$(Egan)IrCH_3$
	$n = 1$	$n = 2$	$n = 1$	$n = 2$	$n = 1$	$n = 1, 2^a$	$n = 1, 2^a$
Distances/Å							
Ir–O*n*	1.973(3)	2.005(3)	1.963(2)	2.017(2)	1.994(3)	2.016(4)	1.994(8)
Ir–N*n*	1.955(3)	1.983(3)	1.946(3)	1.977(3)	1.938(3)	1.938(8)	1.952(8)
Ir–O10	2.031(3)		2.064(2)		5.410(3)	5.462(2), 3.628(2)	4.62(5)
Ir–X	2.3367(10)		2.3534(7)		2.5584(4)	na	2.047(5)
O*n*0–C(*n* + 2)0	1.235(5)	1.191(5)	1.242(4)	1.202(4)	1.194(5)	1.207(4)	1.201(8)
O*n*1–C(*n* + 2)0	1.334(5)	1.344(5)	1.323(4)	1.354(4)	1.340(5)	1.347(3)	1.353(7)
N*n*–C(*n* + 2)2	1.394(5)	1.430(5)	1.396(4)	1.436(4)	1.434(5)	1.416(6)	1.421(6)
C(*n* + 2)0–C(*n* + 2)1	1.474(5)	1.495(6)	1.462(5)	1.495(4)	1.497(6)	1.495(3)	1.497(6)
C(*n* + 2)1–C(*n* + 2)2	1.423(5)	1.395(5)	1.430(4)	1.399(4)	1.400(6)	1.407(5)	1.401(8)
O*n*–C*n*1	1.340(4)	1.325(4)	1.343(4)	1.316(4)	1.329(5)	1.331(6)	1.331(7)
N*n*–C*n*2	1.384(5)	1.357(5)	1.399(4)	1.354(4)	1.394(5)	1.401(7)	1.377(7)
C*n*1–C*n*2	1.421(6)	1.427(5)	1.424(4)	1.426(4)	1.418(5)	1.416(6)	1.420(11)
C*n*2–C*n*3	1.407(5)	1.423(5)	1.398(5)	1.421(4)	1.388(6)	1.396(4)	1.414(6)
C*n*3–C*n*4	1.380(6)	1.359(5)	1.375(5)	1.378(5)	1.395(6)	1.393(4)	1.375(6)
C*n*4–C*n*5	1.402(6)	1.425(6)	1.424(5)	1.427(5)	1.400(6)	1.402(10)	1.421(10)
C*n*5–C*n*6	1.387(6)	1.376(6)	1.384(5)	1.370(5)	1.392(6)	1.396(5)	1.379(6)
C*n*1–C*n*6	1.421(5)	1.414(5)	1.424(4)	1.426(4)	1.402(6)	1.417(8)	1.408(7)
MOS	−1.54(6)	−1.18(10)	−1.53(13)	−1.13(7)	−1.66(9)	−1.66(9)	−1.40(8)
Angles/°							
O1–Ir–O2	86.32(11)		87.15(9)		164.79(16)	171.49(6)	178.79(13)
N1–Ir–N2	170.13(13)		98.96(11)		148.24(17)	167.99(7)	173.86(15)
O*n*–Ir–N*n*	82.59(12)	80.59(12)	83.80(10)	80.21(10)	81.23(13)	80.28(8)	79.82(15)

[a] Values given are the average of chemically equivalent measurements, with estimated standard deviations accounting for both the statistical uncertainty of the measurements and the variance among the chemically equivalent values.

are air-stable and may be separated by column chromatography on silica gel. The compounds are formed in a roughly 4 : 5 : 1 ratio, although the distribution varies from run to run. The paramagnetic compound has an uninformative ^{1}H NMR spectrum, but it is tentatively identified as $(Egan)IrCl_2$ (possibly a mixture of geometric isomers) on the basis of the similarity of its UV-Vis-NIR spectrum (Fig. S22) and EPR spectrum (Fig. S30) to the isomers of $(Diso)_2IrCl_2$.[4]

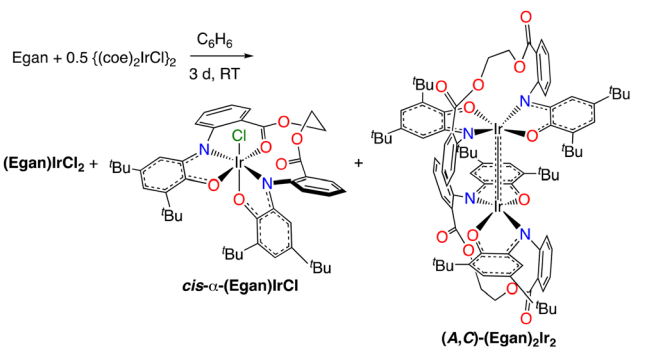

(2)

Preparation, structure, and isomerism of (Egan)IrCl

The major compound isolated from the metalation of Egan is C_1-symmetric, as judged by NMR (for example, all four hydrogens of the CH_2CH_2 bridge are inequivalent). X-ray crystallography indicates that the compound is octahedral, with a chloride ligand and one of the ester carbonyl groups bonded to iridium (Fig. 3). The bridge conformation shares key features with previously observed Egan complexes, including the s-*trans* conformation of the esters and the *gauche* conformation about the CH_2CH_2 linker. To accommodate the 11-membered ring in the novel κ^5 binding mode, the C42–C41–C40–O21 dihedral angle increases to 132.7° compared to values less than 40° seen in previous Egan and Bdan com-

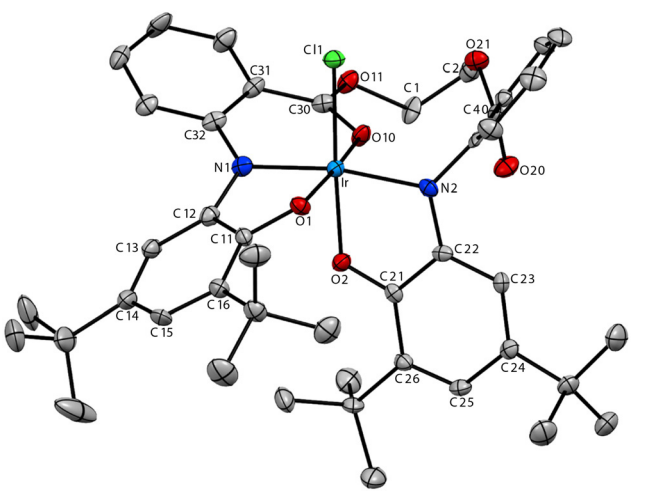

Fig. 3 Thermal ellipsoid plot of *cis*-α-(Egan)IrCl·0.5CH_2Cl_2. Hydrogen atoms, lattice solvent, and minor component of the disordered *tert*-butyl group are omitted for clarity.

plexes. The overall stereochemistry of the octahedral complex is *cis*-α, with the two nitrogen atoms occupying mutually trans sites.

Metal binding of pendant donors on the *N*-aryl substituent of iminoxolene ligands is well precedented, with examples including thioethers,[24] carboxylates,[25] ketones,[26] pyridines,[27] and η^2-alkynes.[28] In these examples, the tridentate ligand is *mer*, as it is in *cis*-α-(Egan)IrCl. The *fac* geometry is accessible, however, as witnessed in piano stool complexes[29,30] or in a triphenylantimony complex.[31]

Octahedral iridium compounds with two *cis* iminoxolenes, a halide, and a neutral donor bound have been reported, and *cis*-α-(Egan)IrCl appears to have a similar electronic structure to these compounds, judging from the similarity of its optical spectrum (Fig. S23) to that of *cis*-$(Diso)_2Ir(py)Cl$.[13] The iminoxolenes show a fold toward the pseudo-twofold axis (average dihedral angles X–Ir–N–C of 122.7°) that is characteristic of *cis* compounds and which minimizes the iminoxolene-Ir π* character of the ligand-centered HOMO.[32]

The degree of electron transfer to iminoquinones can be judged by the intraligand bond distances (Table 2), since these distances are sensitive to the electron density in the iminoxolene redox-active orbital. These distances can be analyzed using established correlations to determine a metrical oxidation state (MOS) for each ligand.[21] The average MOS in *cis*-α-(Egan)IrCl of −1.36 (Table 2) is similar to the average MOS in *cis*-$(Diso)_2Ir(py)Cl$ (−1.22)[13] and to other bis(iminoxolene) iridium monohalides such as $(Diso)_2IrI$ (MOS = −1.32(11)).[4] However, the difference in MOS of 0.36 units between the two iminoxolene ligands in *cis*-α-(Egan)IrCl is unusually large (compare ΔMOS = 0.08 in *cis*-$(Diso)_2Ir(py)Cl$). We attribute the greater degree of reduction of the κ^3-iminoxolene to the ability of the bound ester to act as an effective electron-withdrawing group. *N*-Aryl substituents in iminoxolene ligands typically exert small electronic effects, probably due to the *N*-aryl group being nearly perpendicular to the plane of the iminoxolene ligand.[23] The *mer*, κ^3 binding mode seen in *cis*-α-(Egan)IrCl makes the aryl group more coplanar with the iminoxolene (interplanar angle = 44.5°, compared to 79.5° for the other iminoxolene and anthranilate), and the *ortho* ester substituent, particularly after complexation to iridium, is a good electron acceptor. This ability can be seen structurally in the bond distances, with N1–C32 and C31–C30 bonds significantly shortened, and the C31–C32 and C30–O10 bonds significantly lengthened compared to the corresponding bonds in the κ^2-iminoxolene (Table 2).

Given the elongation of the C=O bond, one would expect to see a significantly decreased carbonyl stretching frequency for the coordinated ester in the IR spectrum of *cis*-α-(Egan)IrCl. In fact, the most striking feature of its IR spectrum is the significant increase in frequency of the uncoordinated ester to 1738 cm^{-1}, compared to 1728 cm^{-1} for (Egan)OsO[8] or 1714 cm^{-1} for (Bdan)Pd.[9] The frequency is calculated by DFT to be 1738 cm^{-1} (on the compound with *tert*-butyl groups replaced by hydrogen), and the hypsochromic shift is tentatively ascribed to ring strain in the 11-membered ring. The coordinated carbonyl is calculated to be strongly bathochromically shifted, absorbing at 1585 cm^{-1}. Experimentally, there is a strong absorption at 1598 cm^{-1}, though the assignment is complicated by the fact that Egan complexes without coordinated carbonyls also have a weak absorption at this frequency. Coordination also induces a downfield shift in the ^{13}C resonance for the ester carbonyl[33] (δ 176.1 ppm *vs.* 168.2 ppm for the free ester or 165.6 ppm for (*E*)-Egan).

cis-α-(Egan)IrCl is stable for prolonged periods at room temperature, but it isomerizes upon heating at 60 °C in benzene (eqn (3)). Equilibrium is achieved over the course of about 3 d at 60 °C, K_3 = 1.7. The product is diamagnetic and can be separated from *cis*-α-(Egan)IrCl by chromatography on silica gel. Its IR spectrum (ν_{CO} = 1746, 1594 cm^{-1}) and optical spectrum suggest that it is six-coordinate with *cis* iminoxolenes and a coordinated ester (δ_{CO} = 187.9 ppm). This is confirmed by X-ray crystallography, which shows a *cis*-β geometry of the iminoxolenes with one *mer*,κ^3-coordinated iminoxolene as in the *cis*-α isomer (Fig. 4).

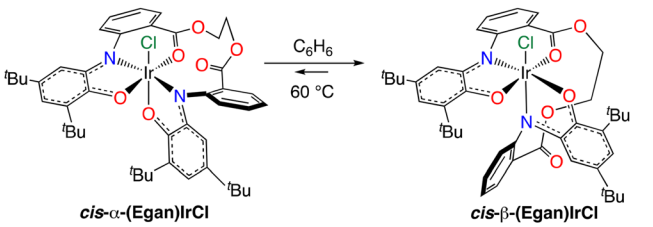

(3)

Evidently the *cis*-α stereoisomer is formed under kinetic control during the metalation reaction. This can be rationalized by the sequence shown in Scheme 1. Binding of one iminoquinone to iridium(I) would likely be followed by rapid displacement of any remaining cyclooctene ligands to form the tridentate complex with a bound ester group. Addition of the

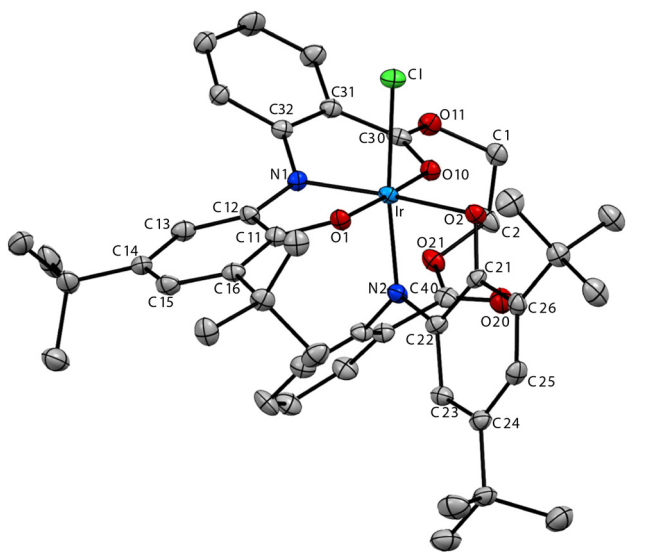

Fig. 4 Thermal ellipsoid plot of *cis*-β-(Egan)IrCl·$(CH_3)_2CO$. Hydrogen atoms and lattice solvent are omitted for clarity.

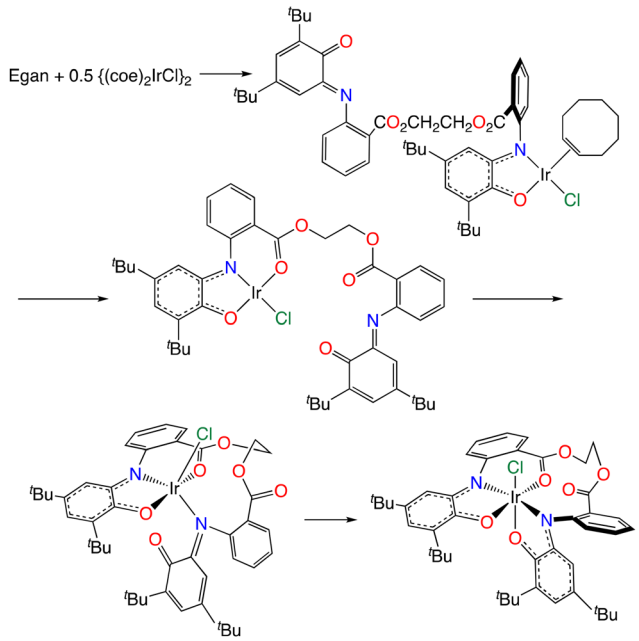

Scheme 1 Proposed sequence of metalation of Egan to form *cis*-α-(Egan)IrCl.

more Lewis basic nitrogen of the second iminoquinone gives a trigonal bipyramidal intermediate that is then poised to form the observed stereoisomer by binding of the iminoquinone oxygen trans to chloride. The thermal isomerization of the *cis*-α stereoisomer to give the *cis*-β stereoisomer is suggested to involve dissociation of the ester carbonyl group, multiple Berry pseudorotations of the five-coordinate intermediate, and rebinding of the ester carbonyl group. This is consistent with the carefully documented mechanism of *trans*–*cis* isomerization in $(Diso)_2Ir(py)Cl$.[13]

Structure and bonding in (*A*,*C*)-$(Egan)_2Ir_2$

The second diamagnetic product isolated on metalating Egan is a species with a single C_2-symmetric Egan environment. Its carbonyl stretching frequency (ν_{CO} = 1731 cm^{-1}) is similar to that of (Egan)OsO, which in combination with the local C_2 symmetry suggests that neither of the ester carbonyl groups is coordinated. The structure of the compound, as determined by single crystal X-ray diffraction, indicates that it is a dimer containing an unsupported iridium–iridium bond (Fig. 5). Because each (Egan)Ir unit is chiral, there are two possible diastereomers of the dimer, but only one is observed. The compound is the (*A*,*C*) stereoisomer,[34] with (crystallographically required) S_4 symmetry.

The most noteworthy aspect of the structure is the short iridium–iridium bond (2.5584(4) Å). This is much shorter than bonds in typical unsupported iridium(II)–iridium(II) dimers,[35] with such distances in neutral complexes averaging 2.74(6) Å (9 examples).[36] Indeed, it is the shortest unsupported Ir–Ir bond of which we are aware. Such a short distance typically requires having at least two one-[37] or two-atom bridges,[38] or at least three three-atom bridges,[39] supporting the metal–metal bond.

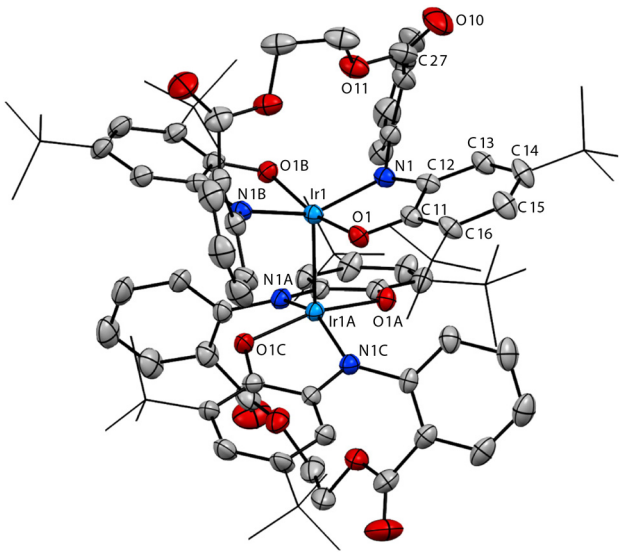

Fig. 5 Thermal ellipsoid plot of (*A*,*C*)-$(Egan)_2Ir_2{\cdot}C_6H_6$. For clarity, hydrogen atoms and lattice solvent are omitted, and *tert*-butyl groups are shown in wireframe.

The origin of the short Ir–Ir bond appears to lie in the π bonding of the complex. The Ir–Ir σ bonding is normal, or if anything is expected to be attenuated due to significant donation of the *B*-symmetry RAO combination into the Ir–Ir σ* orbital (3b orbital, Fig. 6). In the π manifold, there are four pairs of orbitals of *E* symmetry, two sets of dπ orbitals plus the *E* combinations of RAO and SJO orbitals on the iminoxolenes. Because of the relative orientations of the two iridium centers, the d_{xz} orbital on one iridium overlaps strongly with the d_{yz} orbital of the other iridium, and thus all four types of orbitals

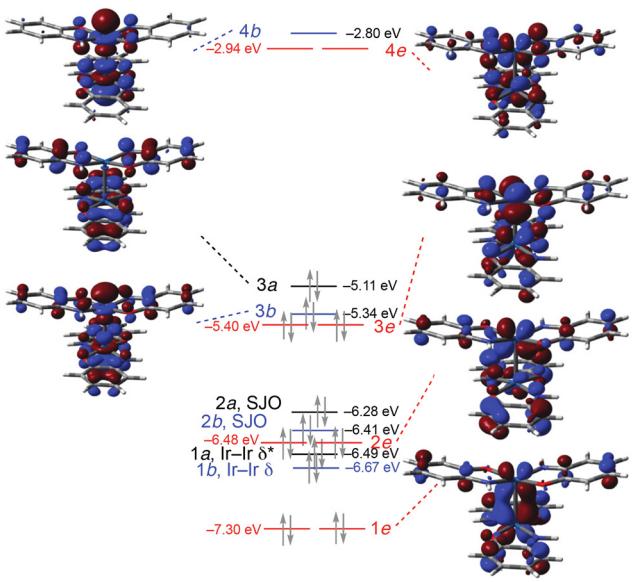

Fig. 6 Partial molecular orbital diagram for (*A*,*C*)-$(Hap)_4Ir_2$ in its lowest-energy (S_4-symmetric) conformation.

mix. The filled lowest-lying orbitals (1e in Fig. 6) are strongly Ir–Ir π bonding, while the empty highest-lying orbitals (4e) concentrate most of the Ir–Ir π* character, though the 2e and 3e orbitals are weakly Ir–Ir π* as well. This leads to a significant net positive π bond order.

If this were an iridium(II) dimer with a non-redox-active ligand, all the dπ orbitals would be filled and there would be no net metal–metal π bonding. Two key features allow the π bonding. First, there is an empty *E*-symmetry pair of orbitals that are predominantly RAO in character (4e in Fig. 6). Such orbitals, along with a filled pair of largely RAO-centered orbitals (3a and 3b in Fig. 6), are characteristic of bis(iminoxolene) iridium complexes and other trans bis-iminoxolene compounds[40] and make the iminoxolenes formally antiferromagnetically coupled iminosemiquinones.[41] The strong interaction of the *E*-symmetry RAO combination with the dπ orbital on each iridium that runs between the iminoxolenes opens a pair of vacant orbitals with significant dπ character. Second, the S_4-symmetric conformation allows the filled metal-centered dπ orbital on one iridium to overlap with this empty orbital. The importance of the orientation is apparent in calculations on (*A*,*C*)-(Hap)$_4$Ir$_2$ (Hap = 1,2-C$_6$H$_4$(NH)O). The lowest-energy conformation of this molecule is calculated to be S_4-symmetric, with a short Ir–Ir bond length of 2.599 Å, in reasonable agreement with experiment. Twisting the structure to a C_{2h} geometry, which abolishes the overlap between the filled and empty π orbitals, results in an increase in free energy of 9.7 kcal mol^{-1} and an increase in bond length to 2.724 Å, typical of an unsupported Ir–Ir single bond.

This analysis does not lend itself to a simple calculation of the iridium–iridium bond order, but one can make a crude estimate by using the metrical oxidation states to gauge the share of the electrons that are on the metal center. The MOS of −1.66(9) gives a nominal Ir oxidation state of +3.34. A redox-innocent Ir^{III,III} dimer would have a metal–metal bond order of 2 and a $\sigma^2\pi^4\delta^2\delta^{*2}\pi^{*2}$ configuration.[39c] This suggests that (*A*,*C*)-(Egan)$_2$Ir$_2$, with its lower population of metal–metal π* orbitals, would have an approximate bond order of 2.34, consistent with the short metal–metal distance.

The optical spectrum of (*A*,*C*)-(Egan)$_2$Ir$_2$ (Fig. 7) is in good agreement with the pattern of absorption predicted by TDDFT for (*A*,*C*)-(Hap)$_4$Ir$_2$, though the calculations predict transitions about 3000 cm^{-1} higher than observed (Table S1). The optical spectra of five-coordinate C_2-symmetric (iminoxolene)$_2$IrX species are dominated by a narrow, intense band in the 700–800 nm region attributed to the transition from the in-phase (*A*-symmetry) RAO combination to the *B*-symmetry Ir-iminoxolene π* orbital as illustrated for example by the spectrum of (Egan)IrCH$_3$ (*vide infra*) in Fig. 7. In (*A*,*C*)-(Egan)$_2$Ir$_2$, there are two such in-phase RAO orbitals (the HOMO and HOMO−1), so this band is split, into a weaker band at 940 nm and a more intense one at 701 nm. In mononuclear compounds, other bands in the visible region would not be especially intense. A number of bands gain intensity in the dimer, for example the 3a → 4b band at 895 nm, the intense 3e → 4e band at 763 nm, and the medium-intensity band at

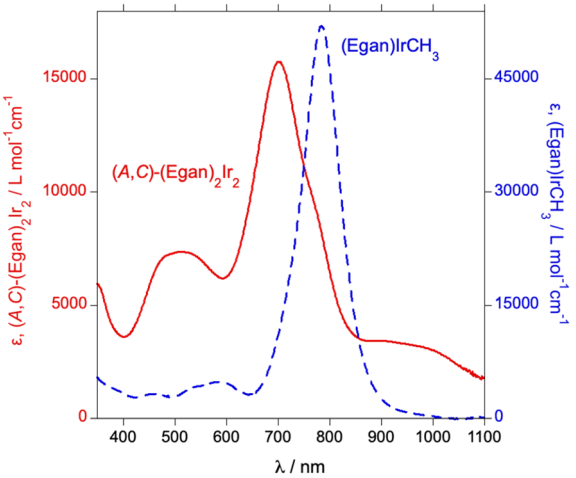

Fig. 7 Optical spectra (CH_2Cl_2) of (*A*,*C*)-(Egan)$_2$Ir$_2$ (solid red line, left axis) and (Egan)IrCH$_3$ (broken blue line, right axis).

513 nm due to excitations from the δ and δ* orbitals (1b and 1a) to the Ir–Ir π* orbital 4e.

Further support for the electronic structure analysis of (*A*,*C*)-(Egan)$_2$Ir$_2$ is afforded by its electrochemistry (Fig. 8). Reduction of the compound is irreversible, but there are four closely spaced reversible oxidation waves in its cyclic voltammogram. This plethora of reversible oxidations is never observed for monomeric compounds and is consistent with the presence of four closely spaced occupied frontier orbitals (3a, 3b, and 3e in Fig. 6).

Overall, metalation of the Egan ligand results in formation of compounds with zero, one, or two chlorine atoms bonded to iridium. This strictly parallels the metalation of the 2,6-

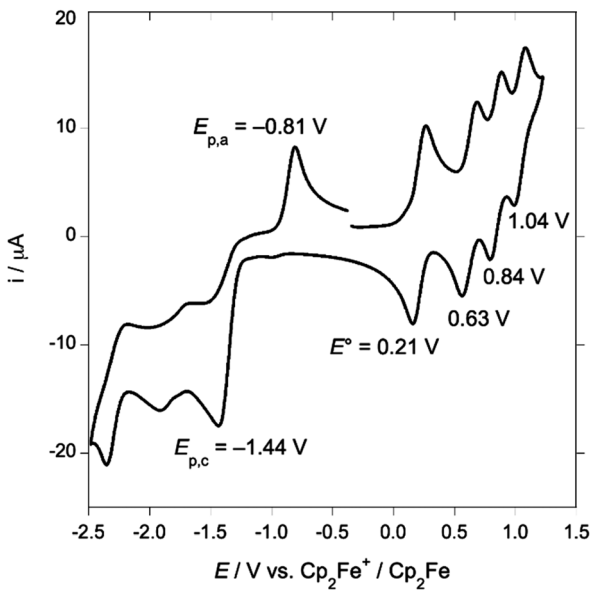

Fig. 8 Cyclic voltammogram of (*A*,*C*)-(Egan)$_2$Ir$_2$ (1 mM in CH_2Cl_2 with 100 mM Bu_4NPF_6, 100 mV s^{-1}).

dibromophenyl-substituted iminoxolene Briq with $\{(coe)_2IrCl\}_2$.[12] Presumably an intermediate in the metalation disproportionates to give (Egan)$IrCl_2$ and the monomeric radical (Egan)Ir (such four-coordinate species are stable with bulkier iminoxolene ligands such as Briq). Dimerization of the radical would afford (*A*,*C*)-(Egan)$_2Ir_2$.

Formation and reactivity of the four-coordinate anion [(Egan)Ir]$^-$

Consistent with the irreversibility of reduction of (Egan)$_2Ir_2$, treatment of the dimer with cobaltocene results in scission of the Ir–Ir bond and formation of four-coordinate [Cp_2Co][(Egan)Ir] (eqn (4)). The same anion is also produced upon reduction of *cis*-α-(Egan)IrCl with excess cobaltocene. (Attempted one-electron reduction of *cis*-α-(Egan)IrCl does not afford (Egan)$_2Ir_2$; the reversibility of the first reduction wave of the monochloride suggests that the reduced species does not readily dissociate chloride.) The anion can be oxidized with ferrocenium ion to regenerate (Egan)$_2Ir_2$.

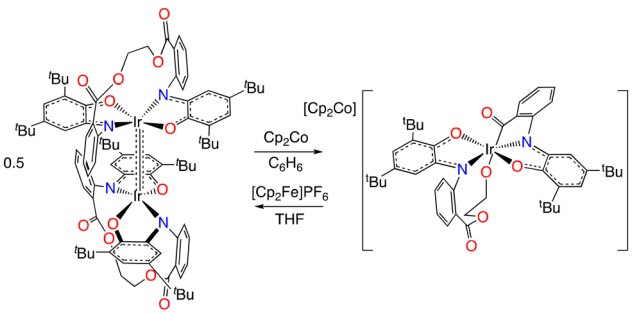

(4)

The structure of [Cp_2Co][(Egan)Ir] (Fig. 9) indicates that the MOS values of the iminoxolene ligands are unchanged from that of (Egan)$_2Ir_2$, consistent with previously observed (iminoxolene)$_2$Ir/[(iminoxolene)$_2$Ir]$^-$ pairs.[12,14] Two structural features do differ from previously observed compounds. First, in contrast to unstrapped bis(iminoxolene)iridium anions, the iridium center is appreciably nonplanar, with an N–Ir–N angle of 167.99(7)°. This distortion is presumably due to the constraints of the diester bridge pulling the nitrogen atoms closer together. A similar deviation from planarity is seen in the analogously strapped (Bdan)Pd.[9] In contrast to the Pd complex, as well as other nonplanar bis(iminoxolene) fragments, which are pyramidalized, in [(Egan)Ir]$^-$ the oxygens are bent away from the nitrogens, so the distortion is toward a tetrahedral geometry rather than toward a square monopyramidal one.

Second, in contrast to other (Egan)- or (Bdan)M complexes, the ethylene bridge is displaced off the twofold axis of the complex. This is likely a solid-state phenomenon that allows the cobaltocenium cation to approach one of the $IrOC_2N$ rings (Co–Ir = 5.42 Å, closest approach to the ligand is Co–C21 = 4.59 Å). This electrostatically favorable contact is seen in unconstrained [Cp_2Co][(Briq)$_2$Ir], which displays a nearly identical ion pair arrangement (Co–Ir = 5.53 Å, Co–C11 = 4.72 Å). The asymmetry in the complex must be highly fluxional in solution, where the anion displays C_2 symmetry in its NMR spectra.

The anion behaves similarly to previously prepared bis(iminoxolene)iridium anions. For example, it reacts rapidly with methyl iodide to give neutral (Egan)$IrCH_3$ (eqn (5)). The neutral methyl complex is air-stable and is structurally (Fig. 10) and spectroscopically very similar to unstrapped analogues (Diso)$_2IrCH_3$ [14] and (Briq)$_2IrCH_3$.[12] Absent the intrusion of the cobaltocenium cation, the ethanediyl strap is again aligned symmetrically, with the compound exhibiting nearly perfect C_2 symmetry. In contrast to the analogous chloride complex, coordination of the ester groups is not observed (ν_{CO} = 1716 cm^{-1}), consistent with the lower Lewis acidity of the methyliridium fragment compared to the chloroiridium fragment. Curiously, the N_2O_2Ir fragment is unusually flat, with N1–Ir–N2 = 173.86(15)° appreciably larger than the angle observed in either (Diso)$_2IrCH_3$ (163.9(8)°)[14] or (Briq)$_2IrCH_3$ (168.21(11)°).[12]

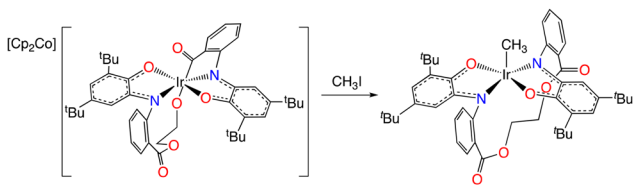

(5)

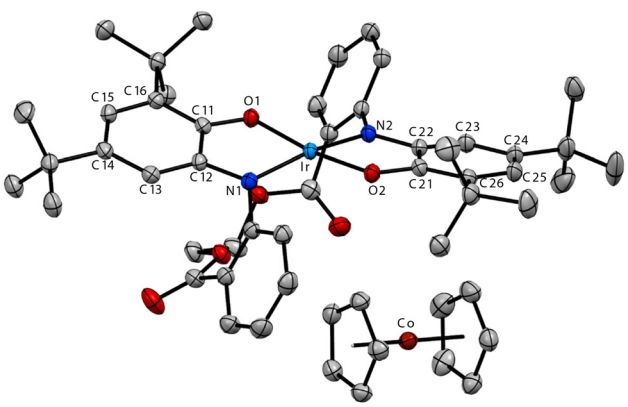

Fig. 9 Thermal ellipsoid plot of [Cp_2Co][(Egan)Ir]·2.5THF. Hydrogen atoms and lattice solvent are omitted for clarity.

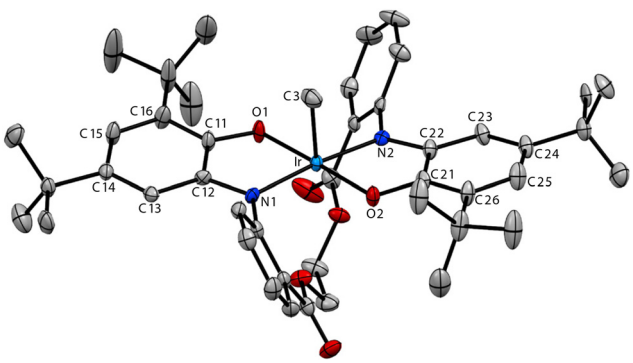

Fig. 10 Thermal ellipsoid plot of (Egan)$IrCH_3$·$2CH_2Cl_2$. Hydrogen atoms, lattice solvent, and the second component of the disordered *tert*-butyl group are omitted for clarity.

Conclusions

The ethanediyldianthranilate-bridged bis(iminoquinone) Egan is metalated by $[(coe)_2IrCl]_2$ to give a mixture of iridium compounds in different oxidation states, analogous to the behavior of the 2,6-dibromophenyl-substituted mono-iminoquinone ligand Briq. Two aspects of Egan give rise to novel features in its coordination complexes with iridium. First, the ester *ortho* to the nitrogen of the iminoxolene can coordinate to the iridium. This results in formation of octahedral iridium complexes with *cis* iminoxolenes, a kinetically formed *cis*-α isomer which thermally equilibrates with the *cis*-β isomer. Second, the low steric profile of the Egan ligand allows a close approach of two iridium centers, so the neutral (Egan)Ir fragment is not observed as a stable monomer, but rather as an iridium–iridium bonded dimer, (*A*,*C*)-$(Egan)_2Ir_2$. This dimer displays a short Ir–Ir bond of 2.5584(4) Å, suggestive of some degree of metal–metal multiple bonding. A molecular orbital analysis indicates that this arises from overlap between the filled metal dπ orbital of one iridium center with the empty Ir–iminoxolene π* orbital of the other iridium that is possible in the observed S_4 geometry of the dimer. The dimer is reduced to a monomeric anion, and methylation of the anion forms five-coordinate (Egan)$IrCH_3$. This chemistry indicates that when the iridium center is electronically predisposed to have a low affinity for other ligands or iridium centers, the bridged bis(iminoxolene) can support chemistry analogous to that supported by unbridged monoiminoxolene ligands.

Conflicts of interest

There are no conflicts to declare.

Data availability

Supplementary information (SI): spectroscopic and computational details. See DOI: https://doi.org/10.1039/d5dt02509e.

CCDC 2490707 (*cis*-α-(Egan)IrCl·0.5CH_2Cl_2), 2490708 (*cis*-β-(Egan)IrCl·$(CH_3)_2CO$), 2490709 ((*A*,*C*)-$(Egan)_2Ir_2·C_6H_6$), 2490710 ((Egan)$IrCH_3·2CH_2Cl_2$) and 2490711 ([Cp_2Co][(Egan)Ir]·2.5THF) contain the supplementary crystallographic data for this paper.[42a–e]

Acknowledgements

This work was supported by the US National Science Foundation (CHE-2400019). H. C. acknowledges support from a Notre Dame College of Science Summer Undergraduate Research Fellowship. We thank Dr Allen G. Oliver for his assistance with X-ray crystallography, and the NSF for support of the acquisition of diffractometers (MRI award CHE-2214606).

References

1 D. L. J. Broere, R. Plessius and J. I. van der Vlugt, *Chem. Soc. Rev.*, 2015, **44**, 6886–6915.
2 R. F. Munhá, R. A. Zarkesh and A. F. Heyduk, *Dalton Trans.*, 2013, **42**, 3751–3766.
3 J. Gianino and S. N. Brown, *Dalton Trans.*, 2020, **49**, 7015–7027.
4 T. H. Do and S. N. Brown, *Inorg. Chem.*, 2022, **61**, 5547–5562.
5 J. L. Boyer, J. Rochford, M.-K. Tsai, J. T. Muckerman and E. Fujita, *Coord. Chem. Rev.*, 2010, **254**, 309–330.
6 J. Cipressi and S. N. Brown, *Chem. Commun.*, 2014, **50**, 7956–7959.
7 T. Marshall-Roth, S. C. Liebscher, K. Rickert, N. J. Seewald, A. G. Oliver and S. N. Brown, *Chem. Commun.*, 2012, **48**, 7826–7828.
8 J. Gianino, A. N. Erickson, S. J. Markovitz and S. N. Brown, *Dalton Trans.*, 2020, **49**, 8504–8515.
9 H. Carbonel, T. D. Mikulski, K. Nugraha, J. Johnston, Y. Wang and S. N. Brown, *Dalton Trans.*, 2023, **52**, 13290–13303.
10 C. Mukherjee, T. Weyhermüller, E. Bothe and P. Chaudhuri, *Inorg. Chem.*, 2008, **47**, 11620–11632.
11 D. D. Swanson, K. M. Conner and S. N. Brown, *Dalton Trans.*, 2017, **46**, 9049–9057.
12 K. Nugraha, T. H. Do and S. N. Brown, *Dalton Trans.*, 2025, **54**, 5896–5905.
13 T. H. Do, D. A. Haungs, W. Y. Chin, J. T. Jerit, A. VanderZwaag and S. N. Brown, *Inorg. Chem.*, 2023, **62**, 11718–11730.
14 M. Meißner, K. Nugraha, K. D. Grandstaff, T. H. Do, C. A. Jiménez, W. Y. Chin, L. E. Farrell, P. D. Nguyen and S. N. Brown, *Organometallics*, 2025, **44**, 760–775.
15 N. G. Connelly and W. E. Geiger, *Chem. Rev.*, 1996, **96**, 877–910.
16 D. Lionetti, A. J. Medvecz, V. Ugrinova, M. Quiroz-Guzman, B. C. Noll and S. N. Brown, *Inorg. Chem.*, 2010, **49**, 4687–4697.
17 M. J. Frisch, G. W. Trucks, H. B. Schlegel, G. E. Scuseria, M. A. Robb, J. R. Cheeseman, G. Scalmani, V. Barone, G. A. Petersson, H. Nakatsuji, X. Li, M. Caricato, A. V. Marenich, J. Bloino, B. G. Janesko, R. Gomperts, B. Mennucci, H. P. Hratchian, J. V. Ortiz, A. F. Izmaylov, J. L. Sonnenberg, D. Williams-Young, F. Ding, F. Lipparini, F. Egidi, J. Goings, B. Peng, A. Petrone, T. Henderson, D. Ranasinghe, V. G. Zakrzewski, J. Gao, N. Rega, G. Zheng, W. Liang, M. Hada, M. Ehara, K. Toyota, R. Fukuda, J. Hasegawa, M. Ishida, T. Nakajima, Y. Honda, O. Kitao, H. Nakai, T. Vreven, K. Throssell, J. A. Montgomery Jr., J. E. Peralta, F. Ogliaro, M. J. Bearpark, J. J. Heyd, E. N. Brothers, K. N. Kudin, V. N. Staroverov, T. A. Keith, R. Kobayashi, J. Normand, K. Raghavachari, A. P. Rendell, J. C. Burant, S. S. Iyengar, J. Tomasi, M. Cossi, J. M. Millam, M. Klene, C. Adamo, R. Cammi, J. W. Ochterski, R. L. Martin, K. Morokuma, O. Farkas,

J. B. Foresman and D. J. Fox, *Gaussian 16, Revision B.01*, Gaussian, Inc., Wallingford CT, 2016.
18 A. P. Scott and L. Radom, *J. Phys. Chem.*, 1996, **100**, 16502–16513.
19 G. M. Sheldrick, *Acta Crystallogr., Sect. A: Found. Crystallogr.*, 2008, **64**, 112–122.
20 *International Tables for Crystallography*, ed. A. J. C. Wilson, Kluwer Academic Publishers, Dordrecht, The Netherlands, 1992, vol. C.
21 S. N. Brown, *Inorg. Chem.*, 2012, **51**, 1251–1260.
22 G. A. Abakumov, N. O. Druzhkov, Y. A. Kurskii and A. S. Shavyrin, *Russ. Chem. Bull.*, 2003, **52**, 712–717.
23 A. N. Erickson and S. N. Brown, *Dalton Trans.*, 2018, **47**, 15583–15595.
24 (*a*) R. Hübner, B. Sarkar, J. Fiedler, S. Záliš and W. Kaim, *Eur. J. Inorg. Chem.*, 2012, 3569–3576; (*b*) S. Maity, S. Kundu, S. Bera, T. Weyhermüller and P. Ghosh, *Eur. J. Inorg. Chem.*, 2016, 3691–3697; (*c*) A. Saha, A. Rajput, P. Gupta and R. Mukherjee, *Dalton Trans.*, 2020, **49**, 15355–15375.
25 (*a*) C. Mukherjee, T. Weyhermüller, E. Bothe and P. Chaudhuri, *C. R. Chim.*, 2007, **10**, 313–325; (*b*) S. Saha, C. R. Choudhury, C. J. Gomez-Garcia, S. Benmansour, E. Garribba, A. Frontera, C. Rizzoli and S. Mitra, *New J. Chem.*, 2017, **41**, 7283–7291.
26 A. V. Piskunov, K. I. Pashanova, A. S. Bogomyakov, I. V. Smolyaninov, A. G. Starikov and G. K. Fukin, *Dalton Trans.*, 2018, **47**, 15049–15060.
27 (*a*) K. S. Min, T. Weyhermuller and K. Wieghardt, *Dalton Trans.*, 2004, 178–186; (*b*) M. A. L. Sheepwash, A. J. Lough, L. Poggini, G. Poneti and M. T. Lemaire, *Polyhedron*, 2016, **108**, 2–7; (*c*) B. Bagh, D. L. J. Broere, M. A. Siegler and J. I. van der Vlugt, *Angew. Chem., Int. Ed.*, 2016, **55**, 8381–8385.
28 D. A. Haungs and S. N. Brown, *Organometallics*, 2022, **41**, 3612–3626.
29 R. Hübner, S. Weber, S. Strobel, B. Sarkar, S. Záliš and W. Kaim, *Organometallics*, 2011, **30**, 1414–1418.
30 M. Bubrin, D. Schweinfurth, F. Ehret, S. Záliš, H. Kvapilová, J. Fiedler, Q. Zeng, F. Hartl and W. Kaim, *Organometallics*, 2014, **33**, 4973–4985.
31 A. I. Poddel'sky, G. K. Fukin and E. V. Baranov, *Russ. J. Coord. Chem.*, 2022, **48**, 902–908.
32 A. N. Erickson, J. Gianino, S. J. Markovitz and S. N. Brown, *Inorg. Chem.*, 2021, **60**, 4004–4014.
33 B. Schreiner and W. Beck, *Z. Anorg. Allg. Chem.*, 2010, **636**, 499–505.
34 N. G. Connelly, T. Damhus, R. M. Hartshorn and A. T. Hutton, *Nomenclature of Inorganic Chemistry IUPAC Recommendations 2005*, RSC Publishing, Cambridge, UK, 2005.
35 S. Wu, S. Zhao, F. Zheng and K. M.-C. Wong, *Inorg. Chem. Front.*, 2025, **12**, 7161–7164.
36 (*a*) P. G. Rasmussen, J. E. Anderson, O. H. Bailey, M. Tamres and J. C. Bayón, *J. Am. Chem. Soc.*, 1985, **107**, 279–281; (*b*) D. M. Heinekey, D. A. Fine, T. G. P. Harper and S. T. Michel, *Can. J. Chem.*, 1995, **73**, 1116–1125; (*c*) H. Hückstädt and H. Homborg, *Z. Anorg. Allg. Chem.*, 1997, **623**, 369–378; (*d*) D. M. Heinekey, D. A. Fine and D. Barnhart, *Organometallics*, 1997, **16**, 2530–2538; (*e*) S. K. Patra, S. M. W. Rahaman, M. Majumdar, A. Sinha and J. K. Bera, *Chem. Commun.*, 2008, 2511–2513; (*f*) H.-P. Lee, Y.-F. Hsu, T.-R. Chen, J.-D. Chen, K. H.-C. Chen and J.-C. Wang, *Inorg. Chem.*, 2009, **48**, 1263–1265; (*g*) H. Huang, A. L. Rheingold and R. P. Hughes, *Organometallics*, 2009, **28**, 1575–1578; (*h*) K. H. G. Mak, P. K. Chan, W. Y. Fan, R. Ganguly and W. K. Leong, *Organometallics*, 2013, **32**, 1053–1059; (*i*) A. L. Rheingold and R. P. Hughes, CSD Communication, 2020, CSD deposition number 2000767.
37 (*a*) H. H. Wang and L. H. Pignolet, *Inorg. Chem.*, 1980, **19**, 1470–1480; (*b*) R. G. Ball, W. A. G. Graham, D. M. Heinekey, J. K. Hoyano, A. D. McMaster, B. M. Mattison and S. T. Michel, *Inorg. Chem.*, 1990, **29**, 2023–2025; (*c*) H. Werner, J. Wolf, A. Nessel, A. Fries, B. Stempfle and O. Nürnberg, *Can. J. Chem.*, 1995, **73**, 1050–1057; (*d*) R. C. Schnabel, P. S. Carroll and D. M. Roddick, *Organometallics*, 1996, **15**, 655–662; (*e*) M. V. Jiménez, E. Sola, A. P. Martínez, F. J. Lahoz and L. A. Oro, *Organometallics*, 1999, **18**, 1125–1136; (*f*) G. L. Moxham, T. M. Douglas, S. K. Brayshaw, G. Kociok-Köhn, J. P. Lowe and A. S. Weller, *Dalton Trans.*, 2006, 5492–5505; (*g*) C. Tejel, M. A. Ciriano, V. Passarelli, J. A. López and B. de Bruin, *Chem. – Eur. J.*, 2008, **14**, 10985–10998; (*h*) S. Shitaya, K. Nomura and A. Inagaki, *Dalton Trans.*, 2018, **47**, 12046–12050; (*i*) Y. Sofue, K. Nomura and A. Inagaki, *Organometallics*, 2019, **38**, 2408–2411.
38 F. A. Cotton and R. Poli, *Organometallics*, 1987, **6**, 1743–1751.
39 (*a*) F. A. Cotton and R. Poli, *Polyhedron*, 1987, **6**, 1625–1628; (*b*) F. A. Cotton, C. A. Murillo and D. J. Timmons, *Chem. Commun.*, 1999, 1427–1428; (*c*) F. A. Cotton, C. Lin and C. A. Murillo, *Inorg. Chem.*, 2000, **39**, 4574–4578; (*d*) M. Ebihara, N. Kanematsu, T. Sakuma, S. Noritake and T. Kawamura, *Inorg. Chim. Acta*, 2005, **358**, 2174–2182.
40 K. M. Conner, A. L. Perugini, M. Malabute and S. N. Brown, *Inorg. Chem.*, 2018, **57**, 3272–3286.
41 P. Chaudhuri, C. N. Verani, E. Bill, E. Bothe, T. Weyhermüller and K. Wieghardt, *J. Am. Chem. Soc.*, 2001, **123**, 2213–2223.
42 (*a*) CCDC 2490707: Experimental Crystal Structure Determination, 2026, DOI: 10.5517/ccdc.csd.cc2plsdh; (*b*) CCDC 2490708: Experimental Crystal Structure Determination, 2026, DOI: 10.5517/ccdc.csd.cc2plsfj; (*c*) CCDC 2490709: Experimental Crystal Structure Determination, 2026, DOI: 10.5517/ccdc.csd.cc2plsgk; (*d*) CCDC 2490710: Experimental Crystal Structure Determination, 2026, DOI: 10.5517/ccdc.csd.cc2plshl; (*e*) CCDC 2490711: Experimental Crystal Structure Determination, 2026, DOI: 10.5517/ccdc.csd.cc2plsjm.